AIAA JOURNAL
Vol. 31, No. 1, January 1993

Shock/Boundary-Layer Interaction Control with Vortex Generators and Passive Cavity

D. C. McCormick*
United Technologies Research Center, East Hartford, Connecticut 06108

This paper describes an experimental comparison of two passive approaches for controlling the shock interaction with a turbulent boundary layer: low-profile vortex generators and a passive cavity (porous wall with a shallow cavity underneath). This investigation is the first known direct comparison of the two methods wherein the advantages and disadvantages of both are revealed. The experiments were conducted with a normal shock wave in an axisymmetric wind tunnel. The shock strength ($M = 1.56$–1.65) was of sufficient magnitude to induce a large separation bubble, thus causing substantial boundary-layer losses. The low-profile vortex generators were found to significantly suppress the shock-induced separation and improve the boundary-layer characteristics downstream of the shock. However, the suppression of the separation bubble decreased the extent of the low total pressure loss region associated with the lambda foot shock system which results in a lower mass-averaged total pressure downstream of the shock. The passive cavity substantially reduced the total pressure loss through the shock system (and thus wave drag) by causing a more isentropic compression over a larger lateral extent. However, the boundary-layer losses downstream of the shock were significantly increased.

Nomenclature

C_f = skin friction coefficient
H = compressible shape factor, δ^*/θ
h = vortex generator height
L = length of passive cavity
M = Mach number
M_o = Mach number upstream of shock
P_{tma} = mass-averaged total pressure
P_{to} = inlet total pressure
P_w = wall static pressure
R = local test section radius
Re = Reynolds number/m, U_∞/ν
$Re_{\delta o}$ = Reynolds number based on boundary-layer thickness, $U_\infty\delta_o/\nu$
U = axial velocity
U_τ = friction velocity
U_∞ = freestream axial velocity
U^+ = normalized velocity, U^*/U_τ
U^* = Van Driest transformed velocity
vg = vortex generator
X = axial distance from converging/diverging nozzle exit
X_s = shock location
X_{pc} = passive cavity leading-edge location
X_{vg} = vortex generator location (downstream tip)
y = vertical distance from wall
y^+ = normalized wall coordinate, yU_τ/ν_w
δ = boundary-layer thickness (based on $0.995U_\infty$)
δ^* = boundary-layer displacement thickness, $\int_0^\delta [1-\rho U/(\rho U_\infty)]\,dy$
δ_o = undisturbed boundary-layer thickness at shock location (that is, smooth wall with no shock or vortex generators present)
ΔX_{pc} = relative shock location for passive cavity, $X_s - X_{pc}$
ΔX_{vg} = relative shock location for vortex generators, $X_s - X_{vg}$
θ = boundary layer momentum thickness, $\int_0^\delta \rho U/(\rho U)_\infty(1-U/U_\infty)\,dy$
ν = kinematic viscosity in freestream
ν_w = kinematic viscosity at wall
ρ = density

Presented as Paper 92-0064 at the AIAA 30th Aerospace Sciences Meeting, Reno, NV, Jan. 6–9, 1992; received Jan. 21, 1992; revision received June 23, 1992; accepted for publication June 24, 1992.

*Research Engineer, Aeroacoustics and Experimental Gas Dynamics Section, 411 Silver Lane. Member AIAA.

Introduction

A NORMAL shock interaction with a turbulent boundary layer occurs in many aerodynamic devices, such as transonic inlets, diffusers, and airfoils, with detrimental effects on drag and pressure recovery. Two passive approaches for controlling the shock interaction are vortex generators and a passive cavity which are shown schematically in Fig. 1. The former method dates back to the early 1950s, shortly after the invention of the vortex generator, where the concept was demonstrated in wind tunnel and flight tests on supercritical airfoils.[1-4] Vortex generators alleviate shock interaction by energizing the low-momentum wall flow in the boundary layer with freestream flow via streamwise vortices, thereby, allowing the boundary layer to negotiate the pressure rise without separation. Note that the lambda-foot structure sketched in Fig. 1a implies some separation is still present since in many cases the vortex generators significantly reduce the size of the separation but do not completely eliminate separation (as was the case in the current investigation). The vortex generators used in this study were not the conventional vane-type devices used in previous investigations, but are low-profile (~ 0.1–0.5δ) wedge-type vortex generators that are the invention of Wheeler.[5] The so-called "Wheeler doublets" are a relatively

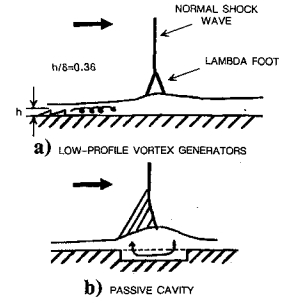

Fig. 1 Passive shock-boundary layer control concepts.

new class of vortex generators that have been shown to alleviate subsonic separation as well as vane-type generators with significantly less parasitic drag.[6] More recent drag measurements of low-profile vortex generators (triangular ramps pointing upstream and downstream) have shown that even for the same height ($h/\delta = 0.4$), conventional vane-type devices possess twice the drag of the low-profile devices.[7] Low-profile vortex generators are attractive for the transonic application because they are submerged in the boundary layer and thus disturb the outer supersonic flow less than vane-type generators (which are typically 1.0–1.2δ). In addition, the wedge geometry is more robust, easier to apply, and, according to the inventor, works over a larger flow incidence range (though the shed vortex array changes from counter-rotating to co-rotating at large incidence angle).

A companion computational analysis of low-profile vortex generators (triangular ramps) and alleviation of shock-induced separation is given by Mounts and Barber.[8] Since the analysis is for an unbounded two-dimensional planar configuration, a direct comparison of their results and the experimental data presented here is not possible. However, strong similarities are observed between the prediction and the experiment which are discussed in more detail in Ref. 8.

The passive cavity concept was suggested by Bushnell and Whitcomb for reducing drag on a supercritical airfoil and experimentally demonstrated by Bahi et al.[9] in the early 1980s. Their encouraging results have led to many experimental and analytic investigations that have been summarized fairly recently by Raghunathan.[10] As shown in Fig. 1b, the pressure rise across the shock induces a passive suction downstream of the shock, which tends to close down the separation bubble, and an injection of flow upstream of the shock. The fluid injection enhances the boundary-layer thickening upstream of the shock, causing a series of compression waves to form (resulting in a more isentropic compression) and the pressure rise to spread over a larger axial distance (which tends to suppress separation). Schlieren photographs of the passive cavity suggest a single oblique shock wave emanates from the leading edge of the cavity in contrast to the series of Prandtl-Meyer compression waves shown in Fig. 1b. This results in a shock structure that looks much like a lambda-foot structure of the solid wall shock-induced separation but much larger in size (for example, see Ref. 9).

The experimental approach for this investigation was to generate a normal shock inside a wind tunnel duct, as opposed to generating a normal shock on a supercritical airfoil. The latter approach has been used for most of the vortex generator and passive cavity studies. The current experiment is a more controlled approach since shock position is located directly with an adjustable downstream plug, and thus the shock position variability of the airfoil approach has been removed from the problem. An axisymmetric test section was selected over a rectangular section in order to avoid the three-dimensional corner interaction that occurs with the rectangular geometry (e.g., see Green[11]).

Experimental Arrangement

The wind tunnel is shown schematically in Fig. 2. Regulated dry air (nominally 10°C total temperature) was introduced

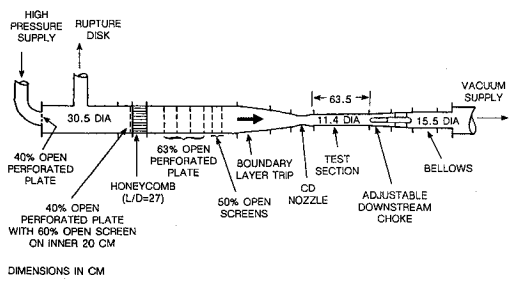

Fig. 2 Schematic of wind tunnel.

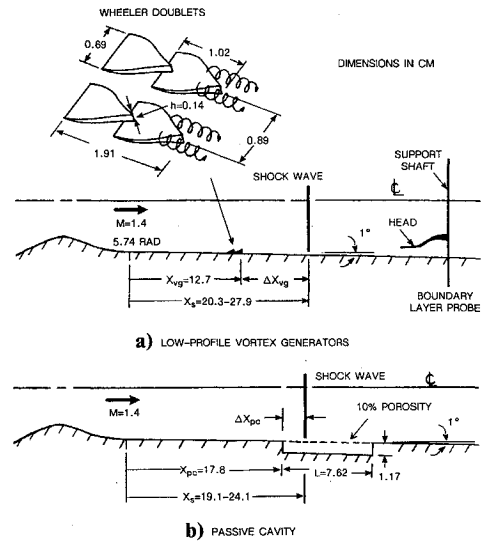

Fig. 3 Experimental arrangement.

into the 30.5-cm-diam plenum where the flow was conditioned with perforated plates, honeycomb, and screens. Downstream of the plenum, the flow was accelerated through a converging/diverging (CD) nozzle (converging/diverging) to $M = 1.4$, the inlet Mach number for the test section. The boundary layer was tripped well upstream of the CD nozzle throat to avoid three-dimensional transition. The test section (11.4 cm inlet diameter and 63.5 cm long) was a machined acrylic conical section that diverged slightly at 1 deg (half-angle) as shown in Fig. 3. Because of this divergence, the Mach number upstream of the shock wave varied in the current experiments from $M = 1.56$ to 1.65, depending on the shock position in the test section ($X_s = 17.8$–27.9 cm). Downstream of the test section, the flow encountered a second choke created by an adjustable plug. The plug position controlled the test section normal shock wave. Downstream of the second choke, the flow entered a Roots blower vacuum system.

Test Section Configurations

The vortex generator arrangement, as shown in Fig. 3a, creates a counter-rotating array of vortices. The doublet generators were installed at the axial location $X_{vg} = 12.7$ cm. The height of the vortex generators was $h = 0.14$ cm and the lateral spacing was 0.89 cm, or 6.4h. The undisturbed boundary-layer thickness (no vortex generators present and shock far downstream) at the vortex generator location was $\delta_{vg} = 0.39$ cm, and thus the height of the vortex generator relative to the boundary layer was $h = 0.36\delta_{vg}$. In addition to this configuration, the upstream wedge of the doublet was removed and a "singlet" configuration was tested to evaluate the merits of the double-wedge arrangement.

The passive cavity arrangement is shown in Fig. 3b. The dimensions of the cavity were 7.62 cm long by 1.17 cm deep, or in terms of the displacement thickness at the start of the cavity, 80δ* long by 12δ* deep. The porosity of the wall was 10% with a hole size of $\delta^*/d = 1.3$. These dimensions and porosity were chosen to be within the range shown to be effective by previous experiments.[10] The passive cavity began at $X_{pc} = 17.8$ cm such that the cavity was approximately located in the shock region where the vortex generators provided the most alleviation (see Fig. 3). In this way, the results from each alleviation method are the most comparable.

Boundary-Layer Measurements

Boundary-layer profiles were measured upstream and downstream of the shock wave with a boundary-layer pitot probe shown in Fig. 3a (tip dimensions of 1.17 × 0.15 mm). The probe spatial resolution was 0.2% of the test section radius (0.15 mm) in the radial or vertical direction from the

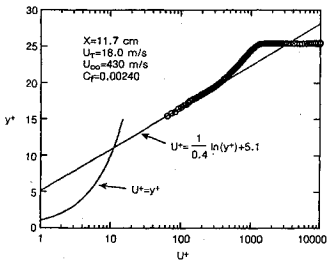

Fig. 4 Law-of-the-wall scaling of inlet boundary layer.

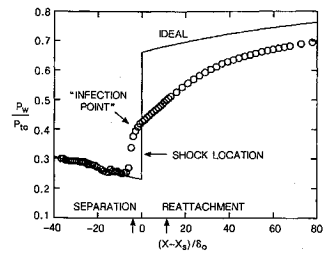

Fig. 5 Baseline wall static pressure distribution.

wall. The support shaft (3.2 mm diameter) of the probe head extended across the diameter of the test section, so that a constant probe blockage was introduced to the flow over the course of a survey. This feature fixed the shock location independent of probe head position. Integral parameters (displacement and momentum thickness) were determined by assuming constant static pressure through the boundary layer at the wall value and adiabatic wall conditions (i.e., constant total temperature). Surveys along different test section diameters (to investigate azimuthal flow variations) was approximated by slightly rotating the probe head about the probe shaft.

Inlet Conditions

The Reynolds number based on conditions upstream of the shock wave was nominally $Re = 1.5 \times 10^7$/m. The undisturbed boundary-layer thickness (that is, smooth wall with no shock present) at the shock location ranged from $\delta_o = 0.46 - 0.58$ cm for the corresponding shock locations $X_s = 17.8 - 27.9$ cm ($X = 0$ is the CD nozzle exit plane). These values give $Re_{\delta o} = 6.8\text{–}8.8 \times 10^4$, which is the relevant Reynolds number for shock-boundary-layer interaction. The profile of the undisturbed boundary layer in law-of-the-wall coordinates (using the Van Driest transformation[12]) indicated a well-behaved logarithmic and wake profile for a turbulent boundary layer as shown in Fig. 4.

Results

Complete data sets (pitot surveys at several axial locations, wall static pressure distribution, and surface flow visualization) were obtained at 4–5 shock wave positions for each case (smooth-wall baseline, the vortex generator, and passive cavity). The complete set of data is presented below in terms of the boundary-layer integral parameters. For brevity, only typical distributions at one shock location are given for static pressure, pitot pressure surveys, and flow visualization.

Baseline

A typical wall static pressure P_w distribution normalized by the inlet total pressure P_{to} for the smooth-wall baseline case is shown in Fig. 5 ($X_s = 20.3$ cm, $M_o = 1.58$). The abscissa in this plot is the distance from the shock normalized by the undisturbed boundary-layer thickness at the shock location (δ_o). The solid line represents the ideal, inviscid flow distribution which is based on the inlet static pressure, shock location, and area variation in the test section. Initially, the data follows the ideal distribution very closely. Just upstream of the shock location, approximately $7\delta_o$, the wall pressure rises rapidly up to the point $(X - X_s) \approx -2\delta_o$ where the pressure gradient suddenly becomes more moderate (labeled "inflection point" in Fig. 5). The pressure increase upstream of $(X - X_s) = 0$ is due to the upstream propagation of the pressure rise through the subsonic portion of the boundary layer. The "inflection point" in the pressure rise corresponds roughly to where the boundary layer separates.[13] Downstream of $(X - X_s)/\delta_o \approx 50 \pm 5$, the pressure distribution begins to parallel the ideal distribution at a depressed level. The lower static pressure value of the actual flow is due to the blockage caused by the considerably thickened boundary layer. The interaction length (axial distance from the initial pressure rise to where the distribution parallels the ideal curve) is approximately $(57 \pm 5)\delta_o$.

The surface flow visualization is shown in Fig. 6 for the same shock location. The visualization technique is a fluorescent tracer/oil flow technique (similar to kerosene/lamp black). The flow is left to right in the photograph. Upstream of the reattachment location, the flow traces moved to the left, or upstream, until they reach the separation location where the pigment builds up and becomes a circumferential ring around the test section. Downstreams of the reattachment location, the flow is downstream in the axial direction. The length of the separation was nominally 6.6 cm or $13\delta_o$. For the range of shock locations $X_s = 17.8\text{–}27.9$ cm, the average separation length varied from 5.8 to 7.1 cm. Scaling these values by the local undisturbed boundary-layer thickness δ_o the separation length was nearly constant with a value of $13\delta_o$.

The boundary-layer development in the test section in terms of the displacement thickness and momentum thickness is

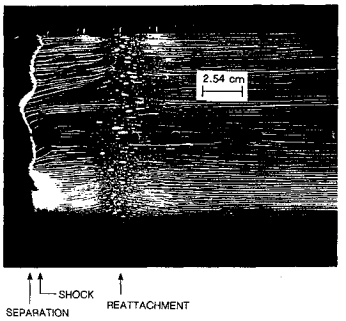

Fig. 6 Baseline surface flow visualization.

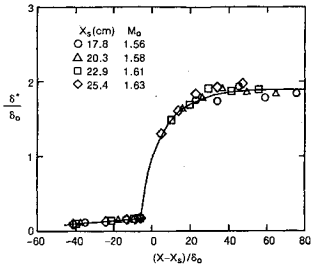

Fig. 7 Baseline displacement thickness distribution.

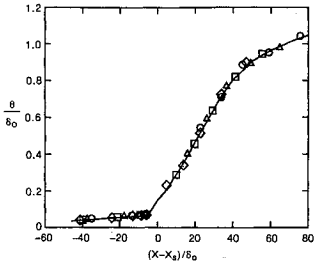

Fig. 8 Baseline momentum thickness distribution.

shown in Figs. 7 and 8, respectively. The abscissa is the normalized distance from the shock and the ordinates have been normalized by the undisturbed boundary-layer thickness. The data in the figures correspond to four shock locations (X_s = 17.8, 20.3, 22.9, and 25.4 cm). In terms of this scaling, the data is seen to collapse onto similarity curves, independent of shock location. This similarity is somewhat surprising since the Mach number upstream of the shock varies from M_o = 1.56–1.63 (in contrast, Kooi[14] reports nonsimilar distributions and a separation length variation of 4.6–10δ_o for a Mach number range M_o = 1.40–1.46). The boundary-layer thicknesses (δ^* and θ) are seen to undergo very large increases typical of strong shock interactions. The corresponding compressible shape factor distribution is shown in Fig. 9. The shape factor starts at approximately the equilibrium value for turbulent M = 1.6 flow (H = 2.4[15]) rises rapidly through the interaction, before relaxing back toward the equilibrium value for M = 0.7 flow (H = 1.5[15]).

It should be noted that the integral parameter estimates near the shock wave [$0<(X-X_s)<20\delta_o$] are somewhat biased due to not accounting for the normal static pressure gradients that exist near shock interactions.

Vortex Generators and Passive Cavity

The vortex generator and passive cavity configurations are compared in terms of the wall static pressure distributions in Fig. 10. The shock location was X_s = 20.3 cm (M_o = 1.58) for all of the data in this figure, and these distributions are typical of other shock locations. For this data, the shock is 55 generator heights downstream of the vortex generators (ΔX_{vg} = 55h), or in terms of boundary layer-thickness, $\Delta X_{vg} = 20\delta_{vg}$. For the passive cavity, the shock position corresponds to $\Delta X_{pc} = 0.33L$. The baseline data is shown as the solid line in the figure. Note that over the porous wall region, no static taps were present.

The vortex generators (circular symbols) are observed to eliminate the "inflection point" in the pressure distribution indicating that the shock-induced separation has been significantly suppressed and thinned. The interaction length (distance from the initial pressure rise to where the distribution parallels the ideal curve) is reduced by a factor of 2.3 from 57 to 25δ_o. The surface flow visualization given in Fig. 11 shows the axial extent of the reversed flow region to be reduced by a similar factor of 2–2.5. The vortex generators are also observed to induce a complicated three-dimensional separation with an "owl-eye" pattern aligned with each vortex generator.

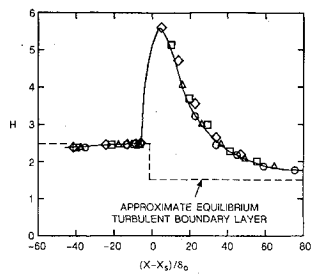

Fig. 9 Baseline shape factor distribution.

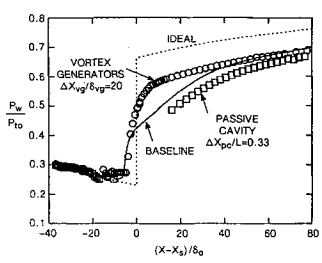

Fig. 10 Wall static pressure distributions.

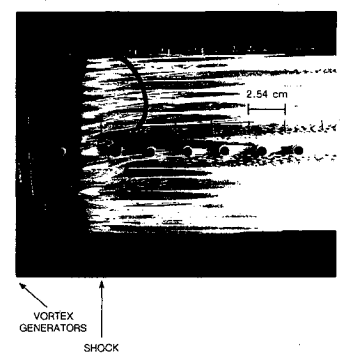

Fig. 11 Vortex generator surface flow visualization, $\Delta X_{vg} = 20\delta_{vg}$.

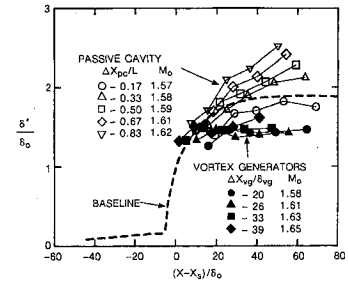

Fig. 12 Displacement thickness distribution.

This surface pattern is similar to the predicted pattern given by Mounts and Barber.[8] Downstream of the shock, the streaks in the surface pattern indicate that the vortices are still coherent and thus continue to energize the boundary layer.

The static pressure distribution for the passive cavity (squares in Fig. 10) is very similar in shape to the baseline case, but depressed in value. The interaction length appears to be somewhat increased. This behavior is consistent with the idea that the passive cavity spreads the pressure rise over a larger axial length. In some ways, the passive cavity is meant to increase the interaction (at least is terms of the length of the pressure rise and the lambda-foot shock system). The depressed value in static pressure relative to the baseline is partially due to the decrease in static pressure rise through the more oblique shock system and partially to the increased thickening of the boundary layer (discussed below).

The boundary-layer characteristics downstream of the shock for the vortex generators and the passive cavity are compared with the baseline distributions in Figs. 12–14 in terms of the displacement thickness, momentum thickness, and compressible shape factor, respectively. The baseline data is represented by the dashed line in the figures (solid line from Figs. 7–9. The vortex generator data for a range of vortex generator-to-shock spacings (ΔX_{vg}) are displayed as the filled symbols and the passive cavity data for a range of positions over the cavity (ΔX_{pc}) are displayed as open symbols. Because of the known three-dimensional nature of vortex generators, different azimuthal locations were surveyed, however, only small variations in the boundary-layer integral properties were observed (a few percent). The scatter in the distributions in Figs. 12–14 are representative of the azimuthal variation since the vortices did not track straight downstream (see Fig. 11) and thus, a set of surveys for a given vortex generator-to-shock spacing correspond to different locations relative to the vortex array.

The vortex generators are observed to cause a decrease in the displacement and momentum thickness by 20–30% for the vortex generator-to-shock spacings of ΔX_{vg} = 20–33δ_{vg}, or 55–97h (Figs. 12 and 13). At 39δ_{vg} the boundary-layer thinning capability of the vortex generators begins to diminish, defining the upper limit on the "range of effectiveness."[4] Note that

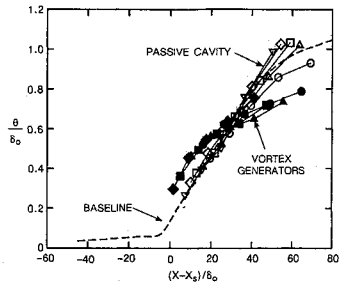

Fig. 13 Momentum thickness distribution.

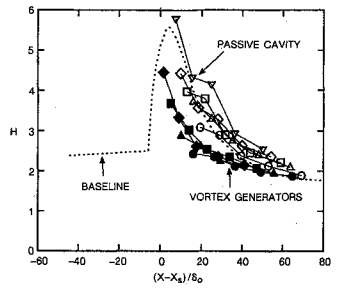

Fig. 14 Shape factor distribution.

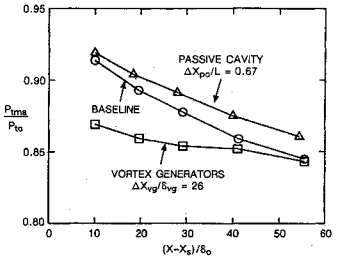

Fig. 15 Mass-averaged total pressure distribution.

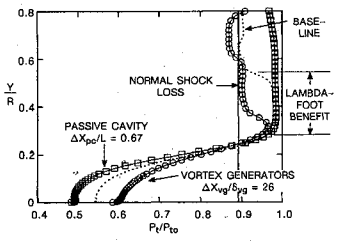

Fig. 16 Total pressure profiles at $(X-X_s)/\delta_o = 20$.

in the range of effectiveness, the boundary layer thinning benefit is nearly constant, independent of ΔX_{vg}. The momentum thickness initially shows an increase over the baseline due to the drag of the vortex generators (Fig. 13). However, the suppression of the separation reduces the flow losses sufficiently to overcome this drag and result in a significant net reduction in boundary-layer losses. The shape factor displays a dramatic reduction in the range of effectiveness of $\Delta X_{vg} = 20\text{–}33\delta_{vg}$ (Fig. 14). In addition to the doublet vortex generator, a singlet configuration was also tested (upstream wedge of doublet removed) to investigate the merits of the double-wedge arrangement. The benefit in boundary-layer thinning (20–30%) was found to be comparable to the doublet; however, the range of effectiveness was somewhat reduced in both the upstream and downstream directions.

In summary, the vortex generators result in a significant thinning of the boundary layer downstream of the shock wave and decreased boundary-layer losses with a considerably healthier (lower shape factor) boundary layer.

The passive cavity, with the exception of the most upstream shock location ($\Delta X_{pc} = 0.17L$), increased the displacement and momentum thickness over the baseline (Figs. 12 and 13). This boundary layer thickening increased with increasing ΔX_{pc}. This trend is due to the increasing length of the porous wall upstream of the shock injecting more fluid which tends to thicken the inlet boundary layer (shock-boundary-layer interaction scales with inlet boundary layer). Also, the downstream porous area providing suction is decreased, reducing the effectiveness at closing down the separation bubble and thereby increasing losses associated with separation. The shape factor also increased over the baseline, indicating that the boundary layer has been significantly aggravated by the passive cavity (Fig. 14). Raghunathan[10] suggests that a relative shock location of $\Delta X_{pc} = 0.67L$ is near the optimum location for a 9% porosity wall. Based on the current results, this location clearly does not correspond to improved boundary layer characteristics. The current boundary layer measurements are consistent with previous passive cavity investigations which observed an increase in viscous losses.[10]

The advantage of the passive cavity is the reduction of the total pressure loss across the shock system that is created by the fluid injection upstream of the shock. This feature is shown in Fig. 15, which plots the mass-averaged total pressure across the test section vs downstream distance for the shock position $X_s = 23$ cm ($\Delta X_{vg} = 26\delta_{vg}$ and $\Delta X_{pc} = 0.67L$). The passive cavity is seen to have the highest mass-averaged total pressure (and thus the lowest shock loss), followed by the baseline and then the vortex generator data. The relatively low total pressure illustrates the primary disadvantage of the vortex generators. However, note that the rate of decrease (mixing losses) is not as rapid as the baseline and the passive cavity due to the healthier boundary layer.

The trend in mass-averaged total pressure is physically explained by Fig. 16 which shows typical surveys of total pressure through the boundary layer (y is normal to the wall). This data was obtained $20\delta_o$ (10.4 cm) downstream of the shock (shock location, $X_s = 23$ cm). The baseline data shown by the dashed line is typical of other shock interaction studies. The region label "lambda-foot benefit" represents the flow from the lambda-foot shock system (shock system due to the large boundary-layer displacement caused by separation) which suffers less total pressure loss than the normal shock value. The vortex generator data (circular symbols) show that the lambda-foot benefit is significantly reduced in radial extent due to the separation suppression (note, the higher wall static pressure and healthier boundary-layer shape). In contrast, the passive cavity significantly enhances the transverse extent of the lambda-foot benefit region (note that the term "lambda foot" is used loosely here since it is not clear if the shock resembles the Prandtl-Meyer compression waves shown in Fig. 1b, or the leading oblique wave more like the lambda-foot shock structure).

The total pressure profiles shown in Fig. 16 show for an axial location of $X - X_s = 20\delta_o$ that the boundary-layer thicknesses for all three cases is about the same. Like the integral thicknesses in Figs. 12 and 13, the thinning of the boundary layer for the vortex generators (and boundary-layer thickening for the passive cavity) appears further downstream. Thus, the suppression of the shock-induced separation does not result immediately in a thinned boundary layer, but rather alters significantly the downstream growth rate.

Conclusions

An experimental comparison has been performed between low-profile vortex generators and a passive cavity for controlling the shock interaction with a turbulent boundary layer. The low-profile vortex generators were found to significantly suppress the shock-induced separation and improve the boundary-layer characteristics downstream of the shock. However, the suppression of the separation bubble decreased the extent of the low-shock loss region associated with the

lambda-foot shock system resulting in a lower mass-averaged total pressure downstream of the shock. The passive cavity substantially reduced the total pressure loss through the shock system by causing a more isentropic compression over a larger lateral extent. However, the boundary-layer characteristics downstream of the shock were aggravated and mixing losses increased. Thus the two methods offer different advantages and disadvantages. For example, if wave drag reduction of an isolated airfoil is required, then the passive cavity approach is probably favored. However, if a supersonic diffuser is the application then the vortex generator approach is probably favored because the shock-induced separation, which usually limits diffuser performance, is suppressed allowing more subsonic pressure recovery to be obtained. The increased pressure recovery should more than make up for the increased shock loss. In conclusion, the approach chosen for shock interaction control should depend on the application.

Acknowledgments

This study was sponsored by Naval Air Systems Command and conducted under the direction of George Derderian (NASC Program Manager) and technical monitor Raymond P. Shreeve (Naval Postgraduate School Technical Monitor). The author wishes to acknowledge their helpful guidance during the performance of the study. The author is especially indebted to Robert W. Paterson of United Technologies Research Center (UTRC) and David E. Hobbs of Pratt & Whitney for their significant contributions to the investigation. Also acknowledged are Gary S. Settles (Pennsylvania State University), William P. Patrick (UTRC), and Gary Wheeler (Vortex Products). Finally, Robert T. Belbin (UTRC) is thanked for his assistance in conducting the experiments.

References

[1]Donaldson, C. P., "Investigation of a Simple Device for Preventing Separation Due to Shock and Boundary-Layer Interaction," NACA RM L50302A, Nov. 1950.

[2]Lina, L. J., and Reed, W.H., III, "A Preliminary Flight Investigation of the Effects of Vortex Generators on Separation Due to Shock," NACA RM L50J02, Nov. 1950.

[3]Powers, W. E., "Application of Vortex Generators for Boundary Layer Control Through a Shock," United Aircraft Research Department Rept. R-95477-6, East Hartford, CT, July 1952.

[4]Pearcey, H. H., "Shock-Induced Separation and Its Prevention by Design and Boundary Layer Control," Pt. IV, *Boundary Layer and Flow Control,* edited by G. V. Lachmann, Pergamon, Oxford, England, UK, 1961, pp. 1167–1339.

[5]Wheeler, G. O., "Means for Maintaining Attached Flow of a Flowing Medium," U.S. Patent 4,455,045, June 1984.

[6]Lin, J. C., Howard, F. G., and Selby, G. V., "Turbulent Flow Separation Control Through Passive Techniques," AIAA Paper 89-0976, March 1989.

[7]Tofanel, S., and Villarreal, R. "Investigation of Vortex Generator Drag," Massachusetts Inst. of Technology, Cambridge, MA, Senior Project 16.622, May 1992.

[8]Mounts, J. S., and Barber, T. J., "Numerical Analysis of Shock-Induced Separation Alleviation Using Vortex Generators," AIAA Paper 92-0751, Jan. 1992.

[9]Bahi, L., Ross, J. M., and Nagamatsu, H. T., "Passive Shock Wave/Boundary Layer Control for Transonic Airfoil Drag Reduction," AIAA Paper 83-0137, Jan. 1983.

[10]Raghunathan, S., "Passive Control of Shock-Boundary Layer Interaction," *Progress in Aerospace Sciences,* edited by A. D. Young, Vol. 25, No. 3, Pergamon, Oxford, England, UK, 1989, pp. 271–296.

[11]Green, J. E., "Interactions Between Shock Waves and Turbulent Boundary Layers," *Progress in Aerospace Sciences,* edited by D. Kuchemann, Vol. 11, Pergamon, Oxford, England, UK, 1970, pp. 235–340.

[12]Maise, G., and McDonald, H., "Mixing Length and Kinematic Eddy Viscosity in a Compressible Boundary Layer," *AIAA Journal,* Vol. 6, No. 1, 1968, pp. 73–80.

[13]Seddon, J., "The Flow Produced by Interaction of a Turbulent Boundary Layer with a Normal Shock of Strength Sufficient to Cause Separation," Aeronautical Research Council, ARC R&M 3502, London, England, UK, March 1960.

[14]Kooi, T. W., "Influence of Freestream Mach Number on Transonic Shock-Wave Boundary-Layer Interaction," National Aerospace Lab., NLR, NLR MP 78013U, Amsterdam, Netherlands, May 1978.

[15]Shapiro, A. H., *The Dynamics and Thermodynamics of Compressible Fluid Flow,* Vol. II, Ronald Press, New York, 1954, p. 1093.